2008

Relating crack heating to vibration for vibrothermography

Christopher J. Uhl
Iowa State University

Relating crack heating to vibration for vibrothermography

by

Christopher Joseph Uhl

A thesis submitted to the graduate faculty

in partial fulfillment of the requirements for the degree of

MASTER OF SCIENCE

Major: Aerospace Engineering

Program of Study Committee:
Stephen D. Holland, Major Professor
R. Bruce Thompson
Jerald M. Vogel

Iowa State University

Ames, Iowa

2008

TABLE OF CONTENTS

LIST OF TABLES iv

LIST OF FIGURES v

ACKNOWLEDGEMENTS vii

ABSTRACT viii

CHAPTER 1. OVERVIEW 1

1.1 Introduction 2

1.2 Calculating Flexural Mode Shapes 5

1.3 Tuning Specimens 5

1.4 Relating Crack Heating to Vibration 6

CHAPTER 2. TUNING SPECIMENS 8

2.1 Theory 9

2.2 Numeric Analysis 12

2.3 Experiment 14

2.4 Comparison of Techniques 16

2.5 Tuning Procedure 18

CHAPTER 3. CRACK DETECTABILITY STUDY 23

3.1 Experiment 23

3.2 Titanium Sample Set 27

3.3 Inconel Sample Set 33

3.4 Conclusion 38

APPENDIX A. ANSYS SCRIPT 39

APPENDIX B. ANSYS RESULTS 40

BIBLIOGRAPHY 41

LIST OF TABLES

Table 2.1 Material properties for titanium and Inconel. (9) 9

Table 2.2 Flexural resonant frequencies of a typical titanium specimen calculated from elementary flexural wave theory neglecting the effect of rotational acceleration. 11

Table 2.3 Flexural resonant frequencies of a typical specimen calculated using Ansys 13

Table 2.4 Change in third order flexural frequency with element size for titanium model. 14

Table 3.1 Hits used for each specimen 24

LIST OF FIGURES

Figure 1.1 Diagram showing test configuration used for ETC study at ISU 4

Figure 1.2 Photograph of laboratory setup used for ETC study at ISU 4

Figure 2.1 Nominal geometry of a specimen from the sample set 9

Figure 2.2 The first three mode shapes calculated from theory. 12

Figure 2.3 Deformed shape of third order flexural mode calculated using finite element analysis. 13

Figure 2.4 Frequency spectrum of titanium specimen. 15

Figure 2.5 This contour plot shows the motion of each point on the surface of the specimen. Zero motion points correspond to flexural nodes. Note that the ends of the sample were not scanned because the clamps are in the way. 16

Figure 2.6 Comparison of experimental, theoretical, and simulated deformed shape of third order flexural mode. 17

Figure 2.7 Change in resonant frequency as a function of specimen length for three samples of differing thickness. 19

Figure 2.8 Histogram showing the distribution of frequencies in the titanium sample set after tuning. 20

Figure 2.9 Histogram showing the distribution of frequencies in the Inconel sample set after tuning. 21

Figure 3.1 Dataguzzler output showing frequency spectrum and IR image. 26

Figure 3.2 Crack heating versus dynamic stress for different crack lengths in titanium, ISU 10/23/07. 28
Figure 3.3 Crack heating versus dynamic stress for different crack lengths in titanium, resonant frequencies only, ISU 10/23/07. 29
Figure 3.4 Crack heating versus crack length for different dynamic stress values in titanium, ISU 10/23/07. 30
Figure 3.5 3D plot of crack detectability data shown with heating versus stress at the front. Titanium, ISU 10/23/07 31
Figure 3.6 3D plot of crack detectability data shown with heating versus stress at the back. Titanium, ISU 10/23/07 31
Figure 3.7 3D plot of crack detectability data shown with heating versus crack length at the front. Titanium, ISU 10/23/07 32
Figure 3.8 Crack heating versus dynamic stress for different crack lengths in Inconel, ISU 02/11/08. 33
Figure 3.9 Crack heating versus dynamic stress for different crack lengths in Inconel taking only hits at resonant frequency, ISU 02/11/08. 34
Figure 3.10 Crack heating versus crack length for different dynamic stress values in Inconel, ISU 02/11/08. 35
Figure 3.11 3D plot of crack detectability data shown with heating versus stress at the front. Inconel, ISU 02/11/08 36
Figure 3.12 3D plot of crack detectability data shown with heating versus stress at the back. Inconel, ISU 02/11/08 36
Figure 3.13 3D plot of crack detectability data shown with heating versus crack length at the front. Inconel, ISU 02/11/08 37

ACKNOWLEDGEMENTS

This material is based on work supported by the Air Force Research Laboratory under Contract #FA8650-04-C-5228 at Iowa State University's Center for NDE.

This material is based on work supported by the Federal Aviation Administration under Contract #DTFA03-98-D-00008, Delivery Order #0037 and performed at Iowa State University's Center for NDE as part of the Engine Titanium Consortium Phase III Thermal Acoustic Studies program.

I would like to take this opportunity to thank Dr. Stephen Holland for his support and guidance on this project; Jeremy Renshaw for sharing his ideas and suggestions over the course of this project; Amelia Doermann and Philip Paschka for helping with lab work and the crack detectability experiments; and the Engine Titanium Consortium for financial support. Finally, I would like to thank my friends and family especially my wife Juli for their understanding and support during this project.

ABSTRACT

Vibrothermography is an inspection technique that detects cracks by observing vibration induced crack heating. Frictional crack heating in a vibrating specimen is directly linked to the resonant vibrational stress on the crack. In simple geometries we can measure the vibrational mode structure and intuit the dynamic vibrational stress field on the crack. This can be used to establish a relationship between crack heating and vibration, which will be critical for vibrothermography to be accepted as a viable inspection technology. We correlate stress to heating by exciting specimens in a well understood and repeatable resonant vibration mode. Through knowledge of the mode shape, a single point surface velocity measurement is sufficient to calculate the deformed shape of the entire specimen. The loads and stresses within the specimen are calculated from the deformed shape and used to identify the relationship between crack heating and vibration. We explore a simplified case of a bar in third order flexural resonance with a surface crack that heats in response to flexure-induced normal load. Specimens are tuned to resonate in third order flexural bending when excited with a single frequency excitation system. We present an observed relationship between dynamic normal stress, crack size, and crack heating.

CHAPTER 1. OVERVIEW

In vibrothermography, a specimen is excited with high amplitude vibration and observed with an infrared camera. The vibration causes cracks to heat through a frictional process (1). Impressive demonstrations provide dazzling pictures of glowing cracks. Vibrothermography has even been shown to detect some cracks that are missed with fluorescent penetrant inspection (FPI) (2). Nevertheless, persistent questions about the reliability and the reproducibility of vibrothermographic inspection have limited its acceptance. In order to widely deploy vibrothermography a more solid physical understanding of the crack heating process is needed. This will permit meaningful extrapolation of crack detectability data to actual parts.

Interest in vibrothermography, also known as sonic infrared or thermosonic nondestructive testing, is motivated by advantages it has over other nondestructive testing (NDT) techniques. Vibrothermography shows substantial promise as an alternative to FPI for turbine components (3). It uses fewer chemicals than FPI, offers greater sensitivity, can be automated, and it can detect cracks under a thermal barrier coating (TBC). These advantages save time, cut cost, and reduce inspector dependence; which leads to more consistent inspections. Vibrothermographic inspections provide a wide field of view that can be adjusted to cover large areas for quick inspections or narrow areas when more detail is needed. This offers an advantage over ultrasound and eddy current where relatively small probes must be scanned over surfaces that vibrothermography can cover with just one image.

This work is part of an effort by the Engine Titanium Consortium (ETC) to quantify crack detectability in engine metals. ETC is a collaboration between Pratt & Whitney, General Electric (GE), Honeywell, and Iowa State University (ISU) organized with the common goal of improving inspection techniques for gas turbines. In essence this project seeks to develop the

test standards, which currently do not exist, for vibrothermography. In many forms of NDT it is sufficient to define a flaw of interest and to apply a particular nondestructive test and record detectability. This sort of hit or miss approach is not sufficient for vibrothermography because detectability is fundamentally tied to the complicated and unique vibration of every part. As a result it may be possible to clearly see a crack indication at one point in a part but a crack of the same size and shape located in a different region of the same part may be invisible. The problem is further compounded by the fact that different parts vibrate in drastically different ways. This means that quantified detectability in one circumstance does not necessarily mean equivalent detection elsewhere.

It is possible to separate vibration variability from crack detectability by accounting for the actual motion of the part (4). Vibration induced crack detectability is a function of crack heating, crack length, and crack motion. In the ideal vibrothermographic inspection crack heating is measured and length and motion values are specified. We make the crack motion a known value by understanding how the crack and the entire part are moving. Resonant modes provide the information required to fully understand the bulk state of stress at any point in the specimen(5). By understanding the vibration of a specimen we remove one of the three unknown products of crack detectability. We can further specify crack length so that heating is observed as a function of motion and crack length. By specifying crack length we set a minimum crack size that will be detectable for a given vibration state. This relationship between the physical quantities of a vibrating crack and the resulting crack heat is the subject of this paper.

1.1 Introduction

Previous studies of vibrothermography have taken a brute force approach to finding defects. These studies excite the test specimen with a high power ultrasonic welder and often rely on nonlinearity in the contact between the specimen and the welder to generate the vibration frequencies necessary to cause crack heating (6). This nonlinear technique can be very effective at finding cracks but it is often very difficult to get repeatable results. Further, the high energy

levels can damage the specimen being tested.

In this study we use tunable excitation which excites the natural motion of the specimen (resonance) so that minimum energy input gives maximum vibration response. By using known resonances, extraction of meaningful and intrinsic information such as the state of stress at the crack is possible. This allows meaningful correlation of the observed crack heating to the properties of the crack motion. By relating the heat generation of a vibrating crack to its properties of motion or state of stress it may be possible to extract a useful relationship that can be used to estimate the detectability of similar cracks in arbitrary parts.

This work uses excitation with a piezoelectric stack in place of an ultrasonic welder. Piezoelectric excitation provides broad band response ranging from 1-30kHz. The use of a tunable excitation source is critical to provide the capability of excitation at resonance. An infrared (IR) camera measures the crack heating and a laser vibrometer measures the motion of the excited specimen. A diagram of this experimental configuration is shown in Figure 1.1. The laser vibrometer measures absolute velocity with respect to time at one point on the surface of the sample. This gives us an accurate velocity history that can be integrated to give displacement for a single point on the sample. The IR camera is calibrated to give absolute temperature measurements over a 640X512 pixel image at 90.9 frames per second. The pneumatic cylinder provides constant coupling force between transducer and sample, and bond paper helps maintain linear coupling. Compliant rubber pins are used to minimize the impact clamping has on the resonant motion of the sample.

This combination of equipment allows the test system to be optimized to a particular specimen. By exciting each specimen at resonance a predictable linear response is possible. A picture of the test setup used at ISU is shown in Figure 1.2.

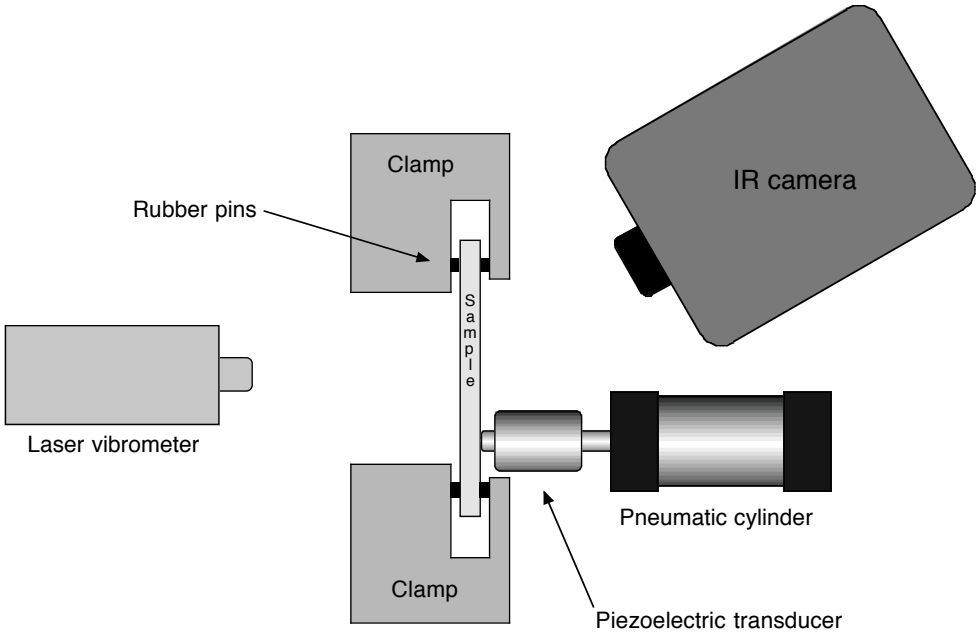

Figure 1.1 Diagram showing test configuration used for ETC study at ISU

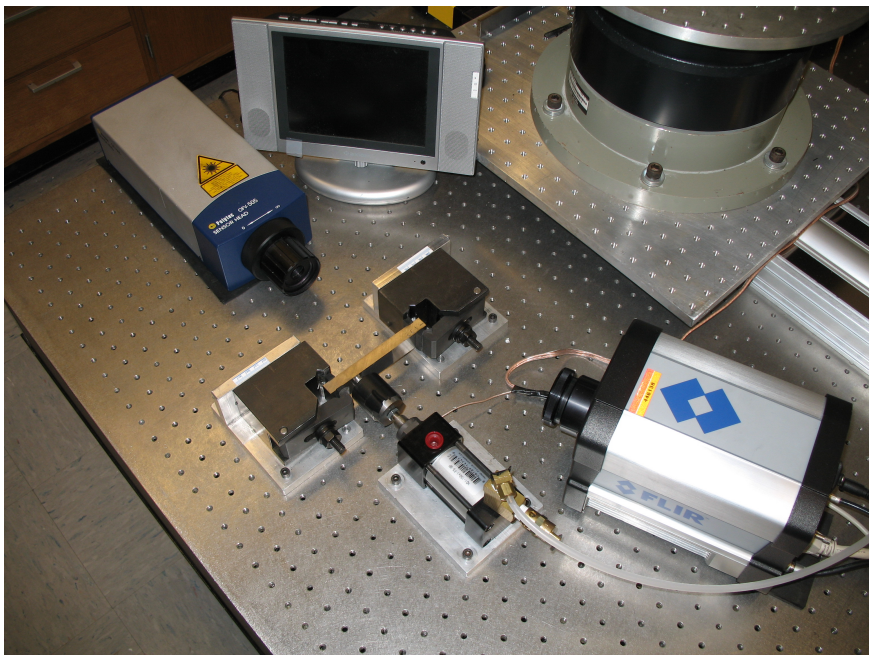

Figure 1.2 Photograph of laboratory setup used for ETC study at ISU

1.2 Calculating Flexural Mode Shapes

In order to understand the state of stress at a crack from a single point vibrometer measurement we must first understand the motion of the entire specimen. Three principal tools are available to provide understanding about the vibration modes present in an arbitrary part. First and most direct is full field measurement which is the displacement measurement of all surface areas on the specimen(7). This has the advantage of providing actual information about the absolute position and motion of the part at any given time(8). We have explored one method of providing full field measurements using a single point laser vibrometer in Section 2.3. Full field measurement is a time consuming process and is not practical for every test which limits its usefulness. Second, finite element simulations estimate the motion of the part; this has the advantage of rapid estimate. Finite element simulations are capable of solving a wide range of specimen geometries but developing models can be a time consuming process. Finally, in cases where the geometry of the part in question is simple enough, theory can be applied to determine the modes of vibration and deformed shapes. Theory is limited to relatively simple geometries.

All of these methods have been explored and will be discussed in Chapter 2. However, elementary flexural wave theory adequately explains the motion of the bar geometry used in this study. In other words by operating at a known flexural resonance it is possible to use a single point vibrometer measurement with flexural wave theory to fully define the deformed shape at any instant in time. In this way the state of stress acting at any point in the specimen can be directly calculated from a single point measurement of vibrometry. This greatly simplifies the measurements required to understand important and fundamental vibration information about the sample.

1.3 Tuning Specimens

With a broad band excitation system it is possible to tune the excitation system to operate at a particular resonance for the specimen being tested. This is an ideal situation because it allows for parts to be tested in multiple resonances. However, not all excitation systems

are broadband. Of the three primary contributors to this project both Pratt & Whitney and GE are using single frequency ultra sonic welders as an excitation source. Thus, a method of exciting samples at a flexural resonance using the single frequency excitation systems was developed. It is possible to tune a particular part so that it resonates at the operating frequency of the excitation system being used. This technique is useful in a laboratory setting where the parts can take any shape you give them. While it is not practical to tune most parts, laboratory samples can be tuned so that the frequency of a particular vibration mode matches the frequency of the excitation source. After tuning, information can be extracted from the single point vibration response because the mode shape is known. Tuning makes it possible to directly compare data from broadband and single frequency excitation systems. In Section 2.5 the process of tuning a sample for excitation at resonance using a single frequency excitation system is explored.

1.4 Relating Crack Heating to Vibration

It is possible to extract a meaningful relationship between crack heating and the state of stress at the crack. A relationship between flexural stress caused by third order bending and heating of the crack will be established. It must be noted that this relationship is not simply one between arbitrary vibration amplitude and heating. Vibration exists in different modes and has different characteristics in each. For example first and third order flexural bending will load a crack located at the center of a rectangular bar in the same way: normal force across the face. However the rate of loading, the bending curvature, and the displacement amplitude will vary depending on the mode and frequency of vibration. For example: First and third mode bending shapes, with equal magnitude displacement at the center of the specimen, will produce different normal stress values. Normal stress caused by bending is a function of the radius of curvature. In a known mode we are able to calculate the radius of curvature from displacement. By considering the actual stresses and frequency of vibration the mode shape is factored out and a better understanding of the crack heat to crack motion relationship is established. This will be considered in more detail in Section 2.1.

In this study we will look at the normal stress generated by a known mode in a relatively narrow frequency band. The calculation of stress is only practical in a known mode because we have no way of connecting the velocity measurements of unknown modes to stresses on the crack. This is why we have taken care to excite these samples in a predictable and linear fashion. Measurements under these conditions provide an extrapolated relationship applicable to samples of arbitrary geometry put under similar dynamic loading (vibration) conditions. Some questions remain unanswered such as the affect of crack closure stresses and individual crack morphology. For cracks produced in the same way, variations in crack closure and morphology are minimum and a correlation between heating and dynamic stress exists.

CHAPTER 2. TUNING SPECIMENS

In this chapter the process used to tune the sample set will be explained. It is important to note that the excitation system used in the Iowa State University lab is broadband thus tuning is not required. We tuned these samples so that after testing in the Iowa State University lab the samples could be sent to partner labs and tested at resonance on single frequency excitation systems. The tuning process we used provides some practical insight about how mode shapes and frequencies change as the sample geometry is changed. Vibration response information from each step during tuning is important because measured results never match theory or simulation exactly. By tuning samples we observe how the vibration changes as the geometry changes. Understanding the range of modes we can tune may help us design future experiments. This is one tool we can use to impose specific stresses on a sample in the vicinity of a crack.

Before tuning any specimens we need an understanding of the resonances that exist in the specimen. The geometry, which controls resonance, of a specimen is given in Figure 2.1. Both the deformed shape and frequency of each resonance must be considered so that a resonance exhibiting the proper characteristics is selected. In this study specimens were sent for testing on an excitation system that used a single frequency 20070 Hz excitation. A vibration mode tunable to 20070 Hz was required in order to excite at resonance. We decided to evaluate the relationship between normal stress, caused by bending, and crack heating because it is relatively easy to excite resonances that cause pure bending. Thus, a mode that loaded the specimen in bending at the point of the crack was required.

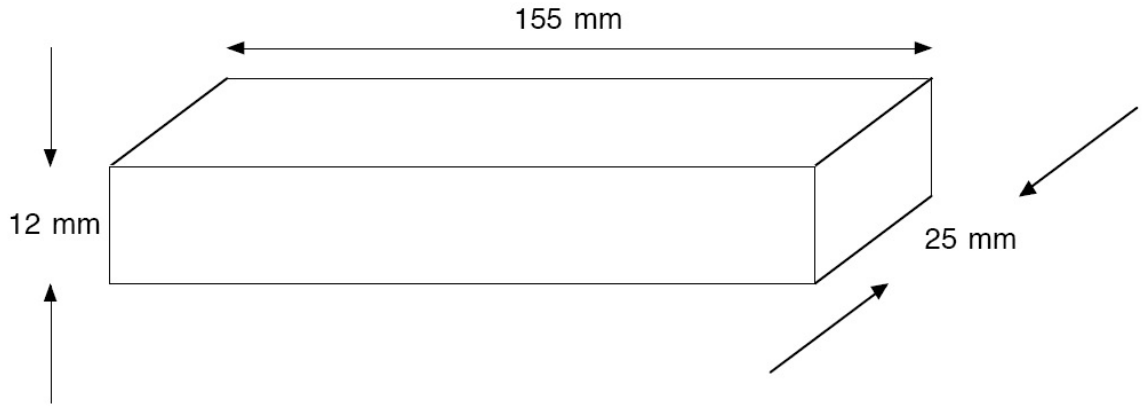

Figure 2.1 Nominal geometry of a specimen from the sample set

2.1 Theory

Because the samples used in this study are of simple rectangular solid geometry we understand their motion using elementary flexural wave theory. Flexural wave theory can provide the deformed shape and frequencies of vibration for each mode. The sample set consists of titanium alloy 6-4 and Inconel® alloy 718 samples for which the material properties are given in Table 2.1. The resonant properties of a particular specimen were calculated using elementary flexural wave theory.

Table 2.1 Material properties for titanium and Inconel. (9)

Material Property	Titanium 6-4	Inconel 718
Density (ρ)	4420 $\frac{kg}{m^3}$	8220 $\frac{kg}{m^3}$
Modulus of Elasticity (E)	105-120 GPa	200 GPa

The wave equation for transverse waves on a uniform slender bar is found by relating the bending moment to the distributed load along the rod (10). When the radius of curvature is large, as we have in the case of this sample set, the bending moment $M(x)$ can be written as

$$M(x) = EI\frac{d^2u(x)}{dx^2}. \tag{2.1}$$

E is modulus of elasticity, I is the second moment of area for the specimen cross section, x is position measured in the length direction, and $u(x)$ is displacement. The distributed load

$w(x)$ is the second derivative of moment and can be written as

$$w(x) = EI\frac{d^4u}{dx^4}. \tag{2.2}$$

In the case where a wave is present there are two inertial loading forces acting on the rod. Most of this force is caused by inertial acceleration in the transverse direction $w_t(x,t)$ and the rest of this force is caused by rotational acceleration $w_r(x,t)$. These forces are given by equation 2.3 and 2.4 respectively where S is cross sectional area and ρ_0 is material density.

$$w_t(x,t) = -\rho_0 S\frac{\partial^2 u}{\partial t^2} \tag{2.3}$$

$$w_r(x,t) = I\rho_0\frac{\partial^4 u}{\partial x^2 \partial t^2} \tag{2.4}$$

The total loading for a free vibration is simply $w(x) = w_t(x,t)+w_r(x,t)$. These samples behave as slender rods so the rotational acceleration term can be neglected resulting in equation 2.5.

$$\frac{d^4u}{dx^4} = -\frac{\rho_0 a}{EI}\frac{\partial^2 u}{\partial t^2} \tag{2.5}$$

Equation 2.5 is an ordinary differential equation with a general solution given by

$$u(x,t) = (A\sinh\kappa x + B\cosh\kappa x + C\sin\kappa x + D\cos\kappa x)\cos\omega t. \tag{2.6}$$

We are using soft rubber pins to clamp the sample so as to approximate a free end clamping condition. Free end conditions will not impose bending moment $\frac{d^2u(x)}{dx^2} = 0$ or shearing force $\frac{d^3u(x)}{dx^3} = 0$ on the vibrating rod. With these boundary conditions applied at $x = -l/2$ and $x = l/2$ the displacement equation and its three spacial derivatives give the ratio of B/D. The resulting equations can be solved for $\kappa_n l = m_n$ where n is the mode number. The values of m_n are given in Reference (10) as

$$m_1 = 4.730 \tag{2.7}$$

$$m_2 = 7.853 \tag{2.8}$$

$$m_3 = 10.996 \tag{2.9}$$

$$m_n = (n + \frac{1}{2})\pi. \tag{2.10}$$

The frequency of the normal mode vibrations is given by

$$\omega_n = \frac{m_n^2}{2\pi l^2}\sqrt{\frac{EI}{a\rho}}. \tag{2.11}$$

The first four modes of vibration are given in Table 2.2.

Table 2.2 Flexural resonant frequencies of a typical titanium specimen calculated from elementary flexural wave theory neglecting the effect of rotational acceleration.

Mode number	Frequency (Hz)
1st	2713.67
2nd	7480.09
3rd	14665.79
4th	24241.57

These are direct calculations using flexural wave theory. From these results we begin to see why the third flexural mode of vibration was chosen for this study. The ultrasonic welders used at Pratt & Whitney and GE operate at 20070 Hz. From Equation 2.11 we see that frequency is inversely proportional to l^2. So as the bar is shortened the frequency of all of the flexural modes will increase. The third flexural mode falls at a frequency that can be easily shifted up to the target frequency and this mode loads the center of the sample with normal force across its face.

The shapes of the first three of these modes are given in Reference (10). These can be calculated from theory by substituting m_n for the appropriate mode number and solving for coefficients A, B, C, and D of equation 2.6. After obtaining these coefficients we substitute back into equation 2.6 and solve over x. The calculated mode shapes are shown in Figure 2.2. Clearly the first and third modes have maximum displacement at the center of the sample while the second mode has a node point at the center. All of the cracks are located at the center of the specimen for this study; this is to say that odd modes put bending load across the crack. Comparison of theoretical mode shape and measured displacement shape is made in Section 2.4.

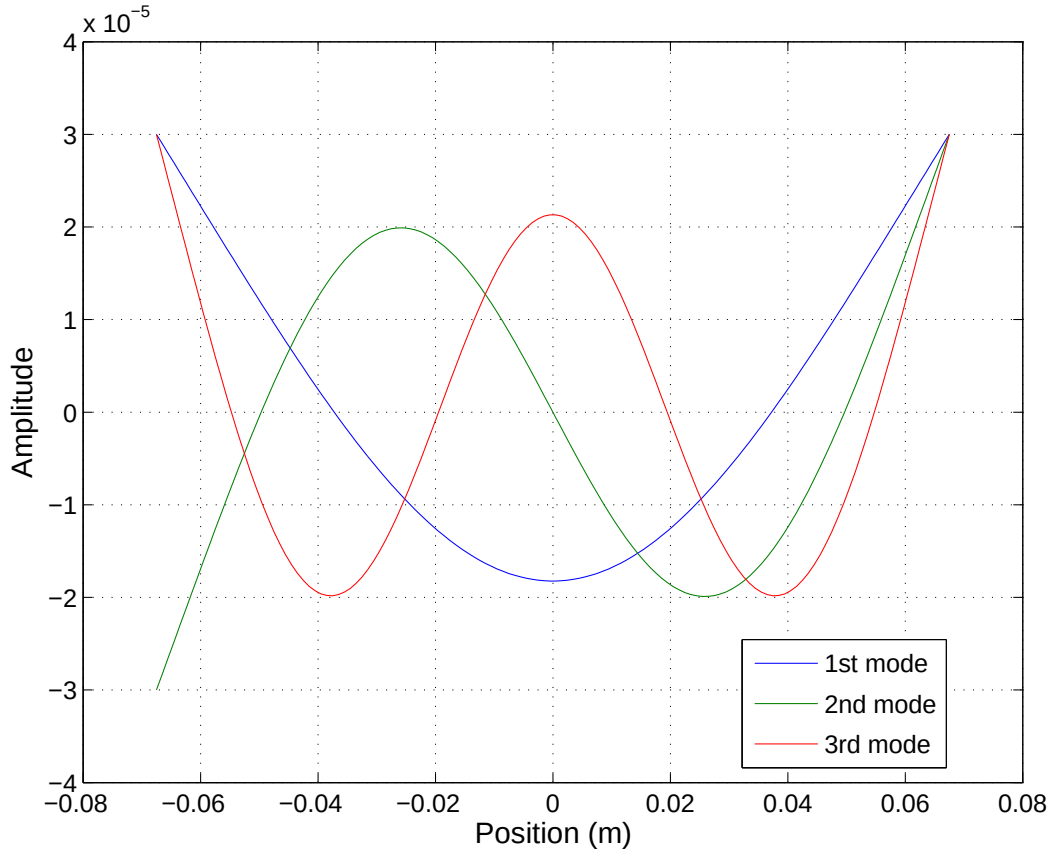

Figure 2.2 The first three mode shapes calculated from theory.

2.2 Numeric Analysis

We calculated the fundamental frequencies of vibration using Ansys, a finite element program. The Ansys script used for these calculations is included in Appendix A. Note that Ansys gives all fundamental modes of vibration where theory only gives flexural (bending) modes. The Ansys output containing the first ten modes of vibration is included in Appendix B. The frequencies of the flexural modes are included in Table 2.3.

A displacement plot from finite element calculations for this specimen is shown in Figure 2.3. A mesh refinement study verified that small enough elements were used to capture third flexural mode frequencies. Mesh refinement is important for modal analysis because as the mode number increases a more refined mesh is required to accurately model the specimen. We tested for convergence by decreasing the element size and recording third order flexural

Table 2.3 Flexural resonant frequencies of a typical specimen calculated using Ansys

Mode number	Frequency (Hz)
1st	2654.4
2nd	7045.2
3rd	13141.0
4th	20491.0

frequency calculated with the new element size. The results are shown in Table 2.4. After looking at convergence data we decided to use a mesh size of 0.004. This was a more refined mesh than required given that less than a .04% improvement over an element size of 0.005 was obtained. Ultimately a mesh size of 0.004 was chosen because it was not time prohibitive to solve and still provided useful frequency information for higher mode numbers.

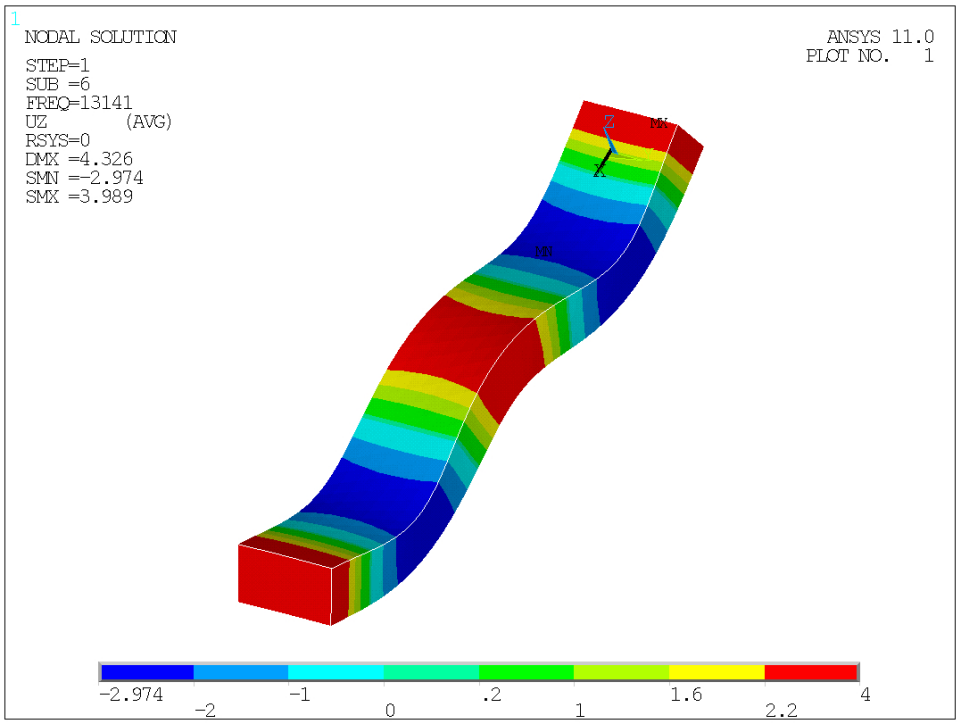

Figure 2.3 Deformed shape of third order flexural mode calculated using finite element analysis.

Table 2.4 Change in third order flexural frequency with element size for titanium model.

Frequency (Hz)	Element size
14069	0.010
13874	0.005
13869	0.004
13867	0.003
13866	0.002

2.3 Experiment

The final method used to understand the deformed shape of these samples was direct measurement. We are limited to single point measurements using a laser vibrometer so a full field measurement at one instant was not possible with our equipment. Instead a low amplitude excitation was used and single point measurements were taken on sequential excitations. Using a low amplitude excitation ensures that contact between the transducer and specimen remains linear. In this way a raster scan of the entire face of the sample was made. Each excitation used the same input sweep and the vibration response of a single point on the sample was recorded. A Matlab script, written by adviser Stephen Holland, was used to evaluate the motion at each point in the scan at the same excitation time step. This makes it possible to observe the absolute velocity of each point on the sample at any time step during the excitation. Displacement is obtained by taking the time integral of velocity.

The frequency spectrum from one excitation is shown in Figure 2.4. The reference spectrum shows spectral amplitude of all frequencies in the specimen. We compare the frequency spectrum with the input function and determine which time step during the sweep resulted in maximum spectral amplitude. We then plotted the deformed shape for that time step.

Because the input sweep is the same for each excitation in the scan the vibration response of the specimen does not change during a scan. In other words the sample will behave in the same way for each excitation. This could be compared to plucking a guitar string. If you pluck the string in the same way you get the same tone from the string. You could continue to pluck the guitar string and measure the displacement at different stations along its length. If

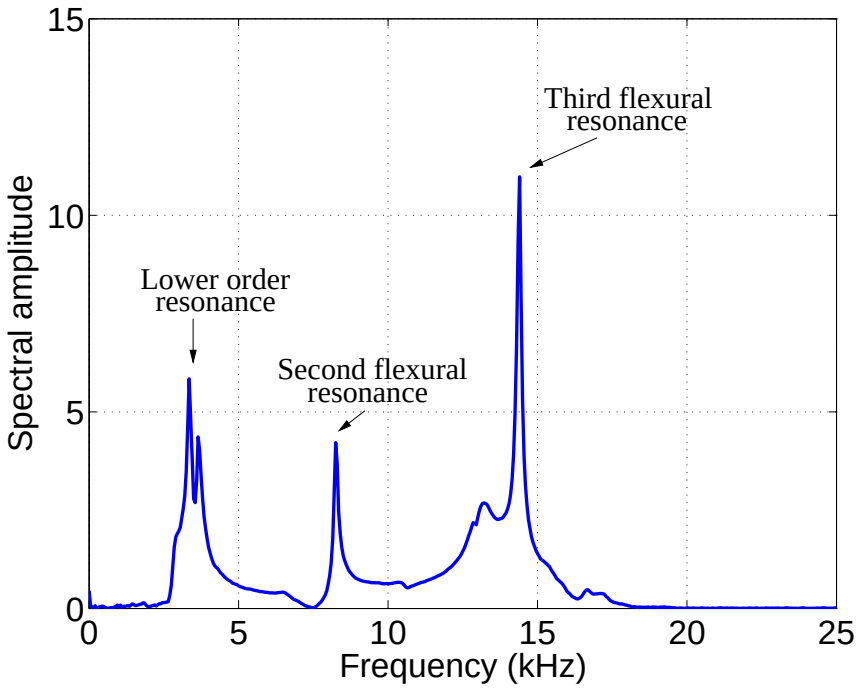

Figure 2.4 Frequency spectrum of titanium specimen.

the plucking was consistent and the displacement measurements were all taken the same time after the pluck they could be combined into one plot of the entire mode shape for the guitar string. In the same way the specimen response is consistent for each excitation; only the point of measurement changes with each excitation. By simply plotting the response at the same timestep of each excitation on a 2D space a contour plot of velocity amplitude is obtained at a particular frequency as in Figure 2.5.

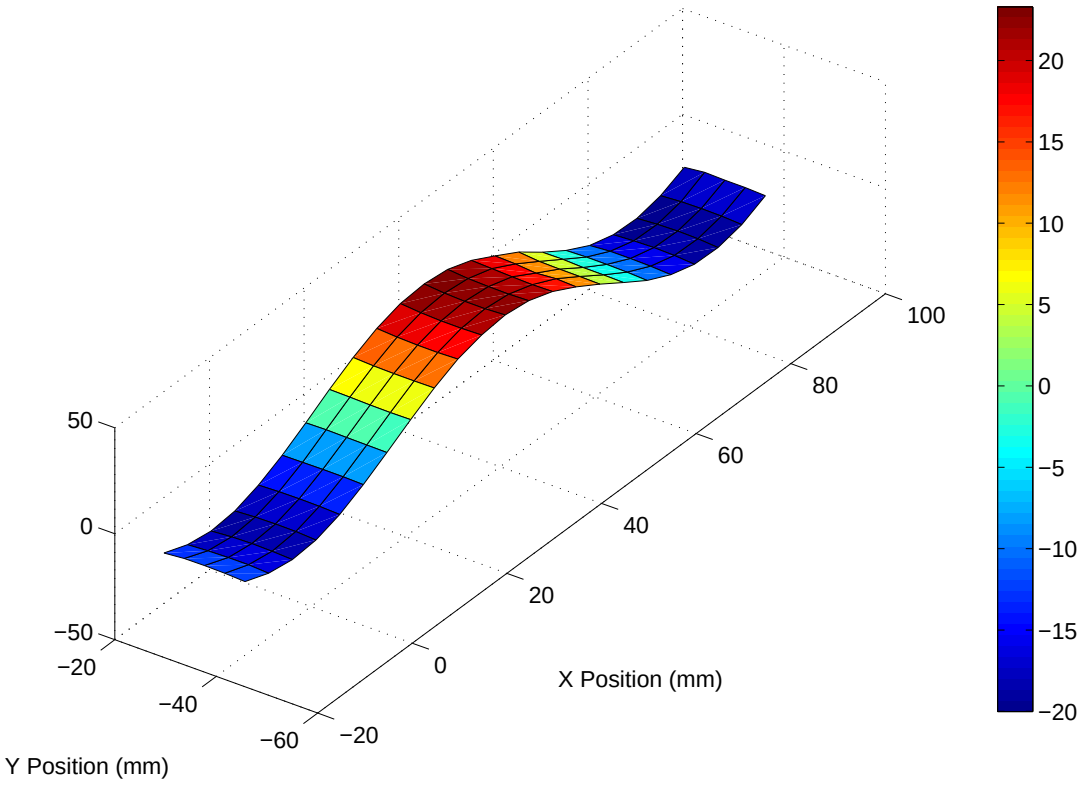

Figure 2.5 This contour plot shows the motion of each point on the surface of the specimen. Zero motion points correspond to flexural nodes. Note that the ends of the sample were not scanned because the clamps are in the way.

2.4 Comparison of Techniques

We used three methods for determining the motion of an excited sample and all three gave the same deformed shape. A direct comparison of theoretical, simulated, and measured profiles is given in Figure 2.6. It is clear from this plot that the three profiles match almost exactly. Mode shape comparisons were made for several titanium and Inconel samples and all produced the same results. Flexural wave theory and simulation match measurement in the range of geometries and material properties that we are working with. With this information it is possible to use a single vibrometer measurement to evaluate the amplitude and frequency of vibration and know the deformed shape of the sample.

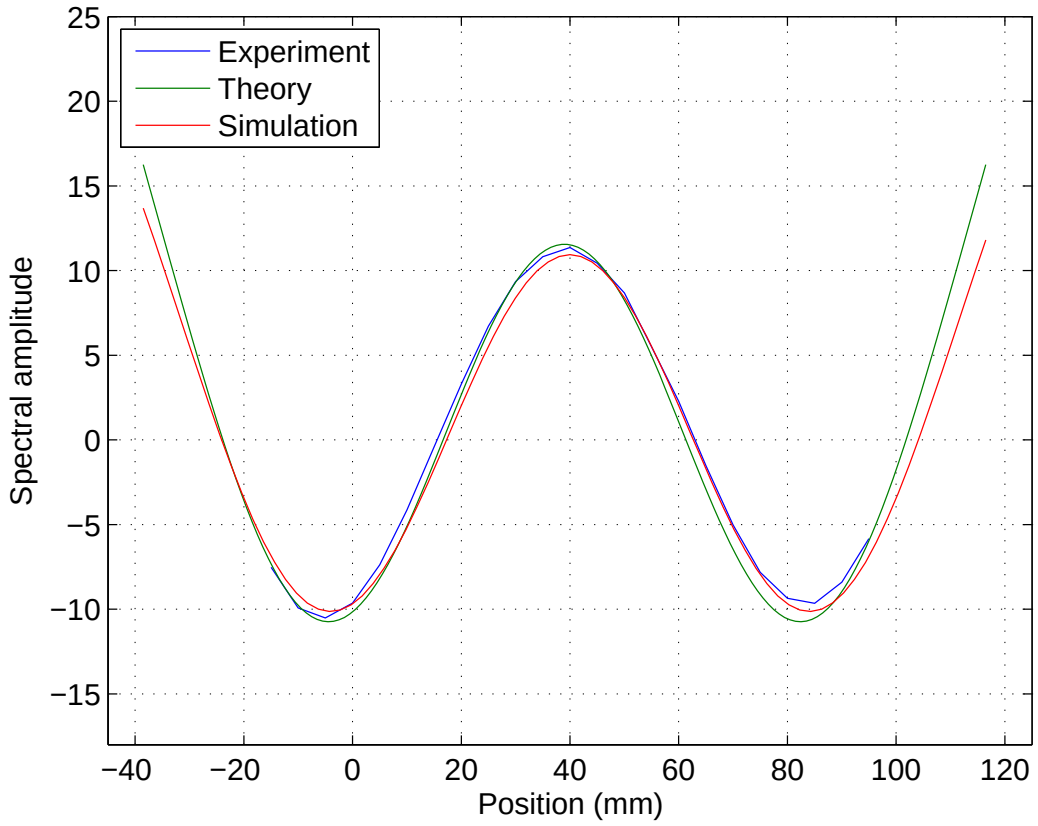

Figure 2.6 Comparison of experimental, theoretical, and simulated deformed shape of third order flexural mode.

When compared to measurement, flexural wave theory tended to overestimate the natural frequencies and finite element simulation tended to underestimate the natural frequencies. Damped natural frequencies are lower than un-damped frequencies and real samples have some natural internal damping. Due to damping we expected to see measured frequencies that were lower than the calculated frequencies. This was the case for theory and measurement but not for simulation and measurement. We began to investigate the error in simulation but we determined that elementary flexural wave theory was sufficient to estimate the deformed shape for these samples. Because theory provided the information we needed to calculate stress we did not continue the study of numeric simulation.

2.5 Tuning Procedure

We understand the deformed shape and natural frequencies of vibration in the sample set using theory, numeric simulation, and measurement. We have decided that normal stress across the crack is the loading mode of interest. Further, we are constrained to modes that exist near 20070 Hz. In the next step we tune specimens in the third flexural mode of vibration because it loads the center of the specimen in bending. We then shift the frequency of the third flexural mode so that it resonates at the same frequency as the ultrasonic welders used as an excitation source at Pratt & Whitney and GE (20070 Hz). The purpose of this tuning procedure is to maintain linear coupling in a pure mode while using a single frequency excitation system. This will allow meaningful comparison of the results obtained in all three labs.

Tuning these samples simply requires changing the geometry until they resonate in the mode of interest at the frequency of interest. Recall that by reducing the length of the specimen the natural frequency of each resonant vibration mode increases. Thus we began tuning the sample set by cutting material off the end of each sample until it resonated in the third mode at 20070Hz. We tuned the first several samples incrementally removing only a few millimeters of material with each step. A resonant frequency measurement provided the information required to extrapolate for the next cut. Figure 2.7 shows frequency change with length for three different samples. After tuning the first few samples incrementally, a relationship between sample thickness and tuned length was used to estimate the tuned length for each of the samples. This relationship is given by Equation 2.12. In the case of titanium the equation is given by 2.13 and for Inconel in Equation 2.14. The $length\ difference$ is the difference in length of the thickest and thinnest specimens in the set after tuning and the $thickness\ difference$ is the difference in thickness of the same two specimens. The intercept is a constant and the $thickness$ is measured for each sample being tuned.

$$target\ length = \frac{length\ difference}{thickness\ difference}(thickness) + intercept \tag{2.12}$$

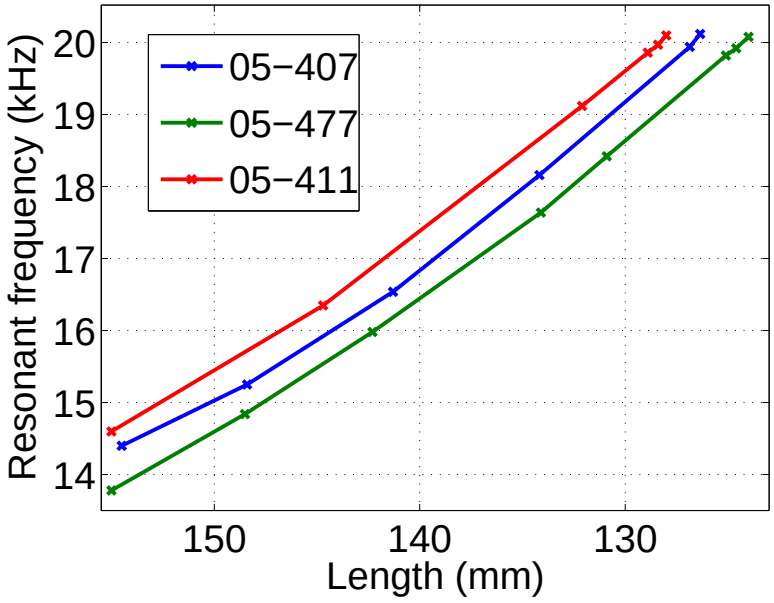

Figure 2.7 Change in resonant frequency as a function of specimen length for three samples of differing thickness.

$$target\ length = \frac{128.09 - 124.04}{13.4 - 12.47}(thickness) + 69.74 \tag{2.13}$$

$$target\ length = \frac{119.89 - 119.6}{12.2 - 12.05}(thickness) + 96.3 \tag{2.14}$$

Equation 2.12 is not a curve fit it is a linear approximation. In order to obtain the resonant frequency versus length slope from Figure 2.7 vibrometer measurements must be taken on the same specimen before and after changing the specimen length. The process of making a cut, measuring frequency, making another cut, and measuring frequency again is very time consuming. Because the range of sample thickness was small we approximated the fit as linear using only the thickest and thinest samples as end points. We tested the linear approximation by tuning additional samples and decided a curve fit would not be required.

By plugging measured thickness into Equations 2.13 and 2.14 we obtain a target length for a sample of measured thickness. Estimating the tuned length by measuring thickness reduced the number of cuts required to tune each specimen. The remaining samples were cut

to length using only two cuts. The titanium samples were tuned first. In order to minimize frequency scatter we intentionally undershot the target frequency. This minimized the number of specimens with frequencies greater than 20070 Hz. After measuring the frequency of the cut samples all samples resonating in the third mode below 20000Hz went back to the shop for additional machining. This process resulted in a relatively tight distribution of frequencies right around the target of 20070Hz as seen in Figure 2.8.

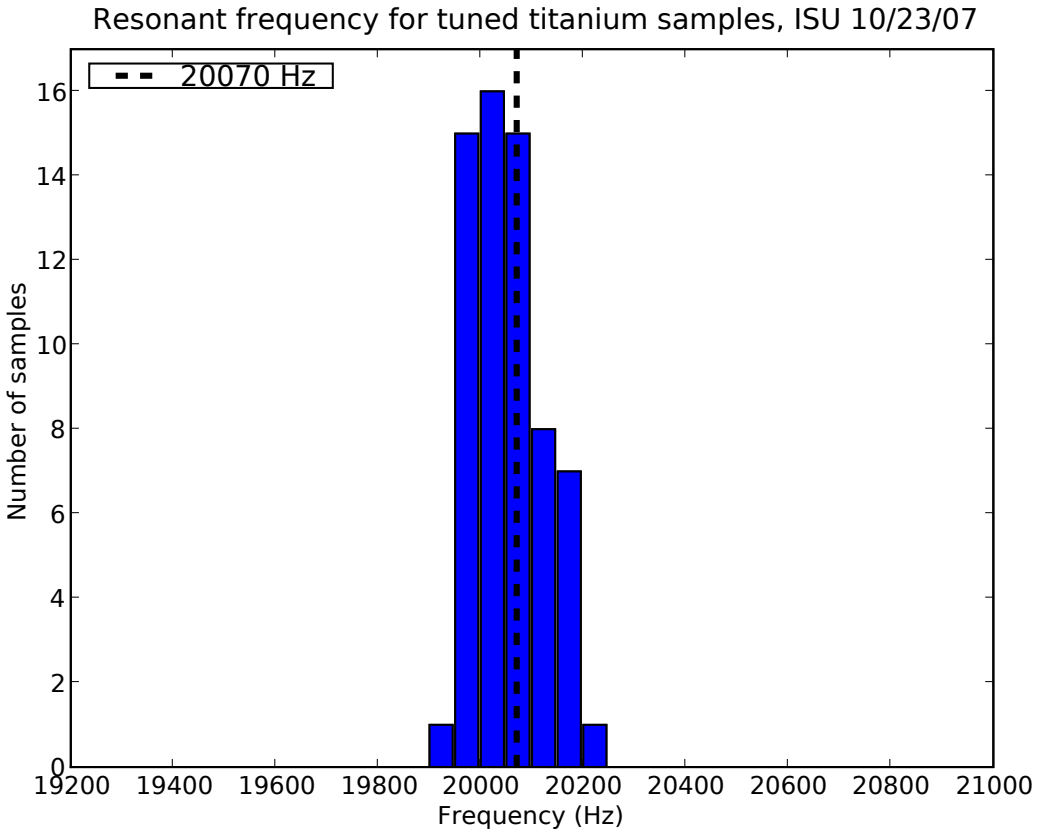

Figure 2.8 Histogram showing the distribution of frequencies in the titanium sample set after tuning.

The process used to tune the Inconel samples was the same except no secondary machining was performed on Inconel samples. The machining of Inconel is cost prohibitive. For this reason the 20070Hz frequency was the target. This resulted in slightly greater scatter of frequencies as shown in Figure 2.9.

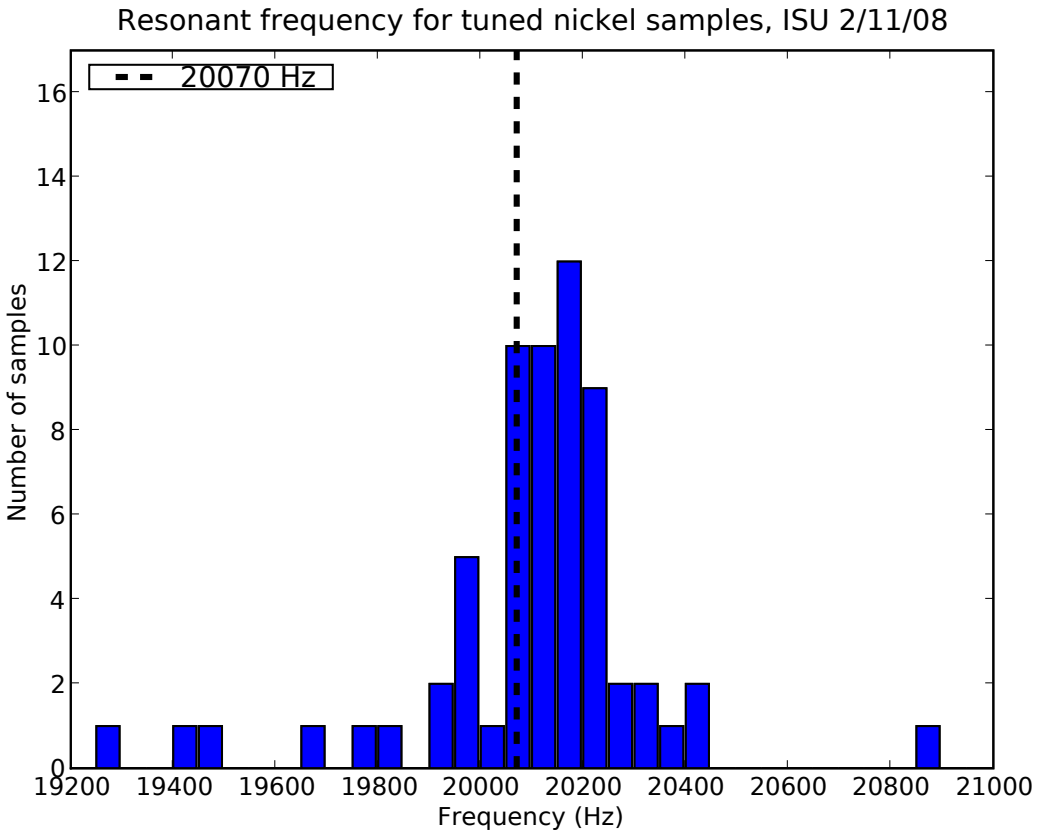

Figure 2.9 Histogram showing the distribution of frequencies in the Inconel sample set after tuning.

The significance of scatter in these resonant frequencies is unclear. We know that when we operate off resonance at ISU using piezoelectric broad band excitation we observe less vibration and lower crack heating. We also know that when we excite well off resonant frequencies we tend to get a much lower response and observe a higher instance of non-linear coupling. This causes chatter between the transducer and specimen which excites a wide range of vibrations. Unfortunately we do not yet have a clear picture of how close to resonance we must be to maintain linear coupling and adequately excite the specimen to cause crack heating. A better understanding will be developed as more information becomes available from partner labs using single frequency excitation. We know that when the specimen is off resonance the measured vibrational stress is lower and as a result we observe reduced crack heating. Thus within the

range of resonances shown in these distributions the effects of being off resonance are accounted for in the dynamic stress to crack heating relationship.

CHAPTER 3. CRACK DETECTABILITY STUDY

After tuning all samples we began a crack detectability study. The intention of this study is not a simple hit or miss analysis. This study was designed to relate crack heating to physical quantities of the crack and vibration process. For the extent of this study we excited the samples in third order flexural resonance. We verified that the dominant frequency present was third order by observing the vibration spectrum.

3.1 Experiment

The Engine Titanium Consortium designed this experiment to compare data between the three primary laboratories involved. The measurement components from all three labs are similar. However, GE and Pratt & Whitney both used single frequency excitation with ultrasonic welders while ISU used a tunable piezoelectric stack as the excitation source. At the time of writing only data from ISU was available for inclusion in this report.

The sample set consisted of 65 titanium and 63 Inconel specimens with low cycle fatigue cracks ranging in length from 20 to 120 mils nominally. Fluorescent penetrant and optical images had already been recorded for all of these samples from a previous study at ISU. Crack lengths were known from this previous study. We tested the entire titanium sample set first and then repeated the procedure with the Inconel sample set.

Samples were cleaned for 60 minutes in acetone then 30 minutes in Photo-Flo® water using an ultrasonic cleaner. Photo-Flo is a surfactant used to helped water penetrate the crack. We intentionally contaminated the crack with water so that paint would not be taken up into the crack. Next, samples were coated with an emissive paint. Then, samples were baked in a dryer at 160 degrees Fahrenheit for 60 minutes to ensure that no water remained in the crack

after painting. Samples were clamped near the flexural nodes using rubber pins at the contact points. Clamping with a compliant material near the nodes minimized the effect clamping had on the specimen resonance. We used paper card stock as a coupling medium between the transducer and the specimen. Finally, a 154N static force coupled the transducer to the specimen. Optimum loading was determined by adjusting the load until maximum vibration was attained. Loading was optimized prior to testing any of the samples recorded in this data set.

We excited each sample seven times. First, a high amplitude frequency sweep set the sample in the clamps. Using the vibration response from the sweep our data collection software determined the exact third order resonance of the sample and automatically recorded it. After determining the resonant frequency samples were hit six more times in a run sequence. Each run sequence consisted of three hits at resonance and three hits at the nominal frequency (20070 Hz). Table 3.1 shows the series of hits used on each specimen. We randomized the order of hits numbered 2 through 7 for each specimen. Randomization prevented error from systemic problems, such as shifting in clamps, that could show up if the same hit order was used each time. Hit amplitudes were selected before the experiment began so that a range of dynamic stresses would be applied. Based on several trial runs we decided that a range of stress from 30 to 100 MPa was ideal. Lower stresses tend not to cause crack heating and higher stress levels were not attainable in this configuration with our excitation system.

Table 3.1 Hits used for each specimen

Randomized	Hit number	Frequency	Amplitude	Titanium	Inconel
No	1	sweep	High	4.0	4.0
Yes	2	resonant	Low	1.5	0.5
Yes	3	resonant	Medium	2.25	1.0
Yes	4	resonant	High	3.0	1.5
Yes	5	20070 Hz	Low	1.5	0.5
Yes	6	20070 Hz	Medium	2.25	1.0
Yes	7	20070 Hz	High	3.0	1.5

For titanium the actual input used arbitrary amplitude settings of 1.5, 2.25, and 3 as the low, medium, and high excitation amplitudes. These do not correspond directly to applied

stress but they are related. Slight variations in the specimens result in a range of stresses even for the same arbitrary amplitude. This is one of the reasons that it is important to relate crack heating to the actual stress and not the excitation settings. In many cases exciting a sample off resonance with an excitation amplitude of 3 will give a lower vibration response than excitation at resonance with a vibration amplitude of 1.5. By relating crack heating to stress instead of input power we can factor out variations in the excitation response.

The low, medium, and high settings are different for titanium and Inconel. There are two reasons for using different excitation input amplitudes. First, the impedance mismatch between the transducer and specimen is different for each metal. Differences in impedance cause different feedback into the transducer which changes the arbitrary excitation amplitude required to couple energy into the specimen. Second, a different transducer was used for each sample set. We started with a relatively new transducer for each experiment in order to minimize the chance of transducer failure during testing. The transducers and excitation settings were picked based on the range of stresses they could excite in each metal and the transducer used for the Inconel was slightly different than the one used for titanium.

We used a custom software package "dataguzzler" to capture waveforms and images. This software allows real time processing of the captured waveforms and images so that background subtraction, Fourier transforms, and math operations can be applied to captured data. A typical screen shot showing an IR image and frequency spectrum for one sample is shown in Figure 3.1. Vibrometer signal and IR data is collected and saved for each hit.

Bending stress, calculated from theory, is given at the surface of a specimen loaded in bending by Equation 3.1. Where M is bending moment, $h/2$ is the distance from the neutral axis (half thickness), and I is the second moment of area for the specimen cross section.

$$\sigma_{xx} = \frac{Mh}{2I} \tag{3.1}$$

Recall that moment is given in Equation 2.1. Thus, bending stress can be rewritten using Equation 2.1 as

$$\sigma_{xx} = \frac{Eh}{2}\frac{d^2u(x)}{dx^2}. \tag{3.2}$$

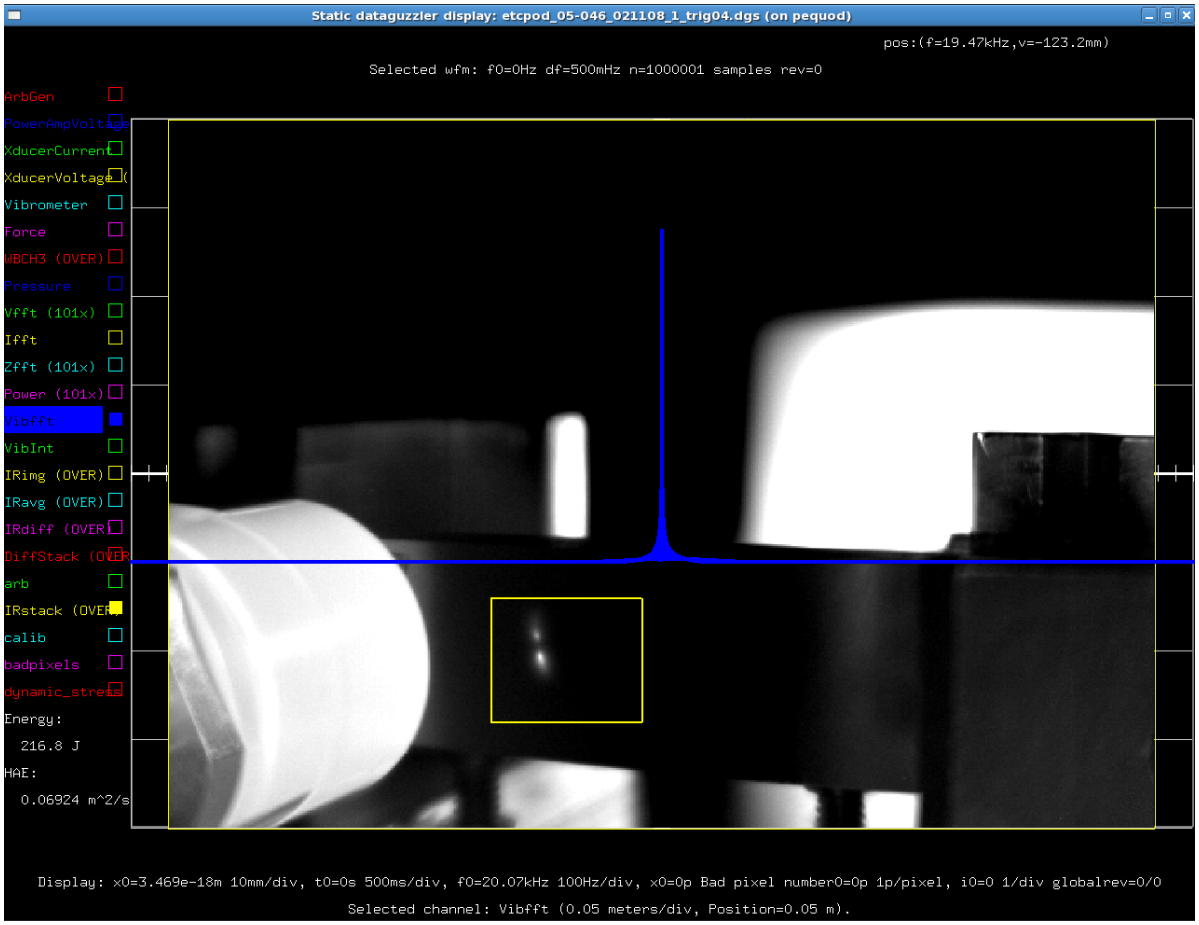

Figure 3.1 Dataguzzler output showing frequency spectrum and IR image.

It can be shown that for symmetric modes coefficients A and C from Equation 2.6 are zero and the ratio of $\frac{B}{D}$ is given by

$$\frac{B}{D} = \frac{\cos \kappa l/2}{\cosh \kappa l/2} (\text{symmetric modes only}). \tag{3.3}$$

Substitution of $\frac{d^2u(x)}{dx^2}$ into Equation 3.2 gives

$$\sigma_{xx} = \frac{Eh}{2} \kappa^2 \left(B \cosh \kappa x - D \cos \kappa x \right) \cos \omega t. \tag{3.4}$$

Substitution of the ratio $\frac{B}{D}$ results in

$$\sigma_{xx} = \frac{DEh}{2} \kappa^2 \left(\frac{\cos \kappa l/2}{\cosh \kappa l/2} \cosh \kappa x - \cos \kappa x \right) \cos \omega t \tag{3.5}$$

which gives stress as a function of x and t for symmetric modes. Evaluated at the center of

the sample ($x = 0$) Equation 3.5 becomes

$$\sigma_{xx} = \frac{Eh}{2}\kappa^2 \left(\frac{\frac{\cos \kappa l/2}{\cosh \kappa l/2} - 1}{\frac{\cos \kappa l/2}{\cosh \kappa l/2} + 1} \right) u \Bigg|_{x=0} . \tag{3.6}$$

For third order flexural bending $\kappa l = m_3 = 10.996$ (from Equation 2.10). Thus $\kappa l/2 = 5.498$ and the term in parentheses is $-.98848$. So for third order flexural bending the stress caused by dynamic loading is given by

$$\sigma_{xx} = \frac{Eh}{2}\frac{10.996^2}{L^2}(-.98848)u \Bigg|_{x=0} \quad \text{(3rd order flexural only).} \tag{3.7}$$

Equation 3.7 was used to calculate the bending stresses for each excitation where E, h, and L are known and u is the integration of the vibrometer signal.

An algorithm written by Steve Holland was used to determine the crack heating. This algorithm determined the area of the crack and the temperature of each pixel then integrated to get a heating value. This heating value was then divided by area to give a temperature. Using a computer program to measure the crack heating gave more consistent results between inspectors. All of the heating values recorded here have been automatically generated.

3.2 Titanium Sample Set

Titanium samples were tested in one batch before the Inconel samples. Figure 3.2 shows dynamic stress versus crack heating for all of the titanium samples. Points that fall below the dotted line (30mK) are below the detectability threshold. The noise threshold for our camera is 20mK. It is clear that higher dynamic stress values cause higher crack heating values. We also see that larger cracks heat more.

There are a significant number of points clustered in the low stress area (left) of Figure 3.2. At first glance this seems to be cause for concern. Given the distribution of low, medium, and high amplitude excitations we expect to see an even distribution of stress values. The reason for bias toward lower stress values is because not all of the samples were tuned exactly to the nominal frequency. Off resonant excitations do not to vibrate the samples very well. As a result, when the resonant frequency is more than 10-15 Hz from nominal we observe a drop in dynamic stress.

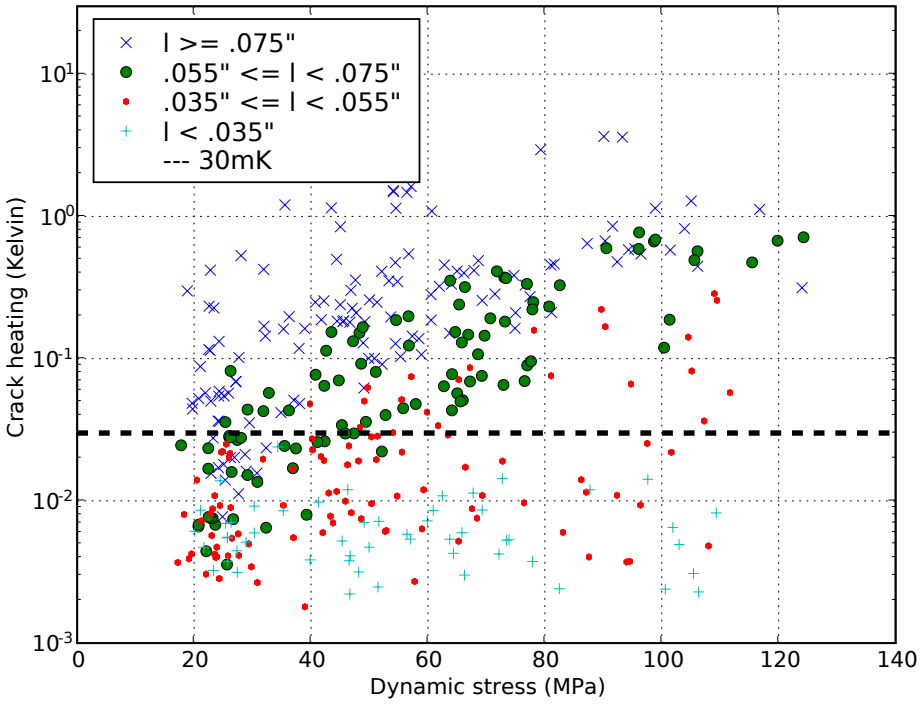

Figure 3.2 Crack heating versus dynamic stress for different crack lengths in titanium, ISU 10/23/07.

Half of the excitations were at the nominal frequency of 20070 Hz. Samples that resonated off the nominal frequency resisted excitation at nominal frequency. This caused less efficient energy input to the sample and resulted in less vibration. When only the resonant frequency vibrations are plotted (Figure 3.3) we see the distribution of stresses we expected to see. Figure 3.3 shows less clustering of points at the low end of the stress scale because the nominal frequency excitations have been removed. The careful observer may also note that there are also fewer points in the high stress range. Figure 3.3 has all nominal frequency hits removed. Some of the samples were tuned very close to the nominal frequency. Samples with resonance near 20070 Hz experience high amplitude vibration with nominal frequency excitation.

In both Figures 3.2 and 3.3 we see that crack heating is tied to crack size and stress. Small cracks remain undetectable at higher stress levels. We also observe that large cracks are not detectable with inadequate stress. This suggests that there is some minimum amount

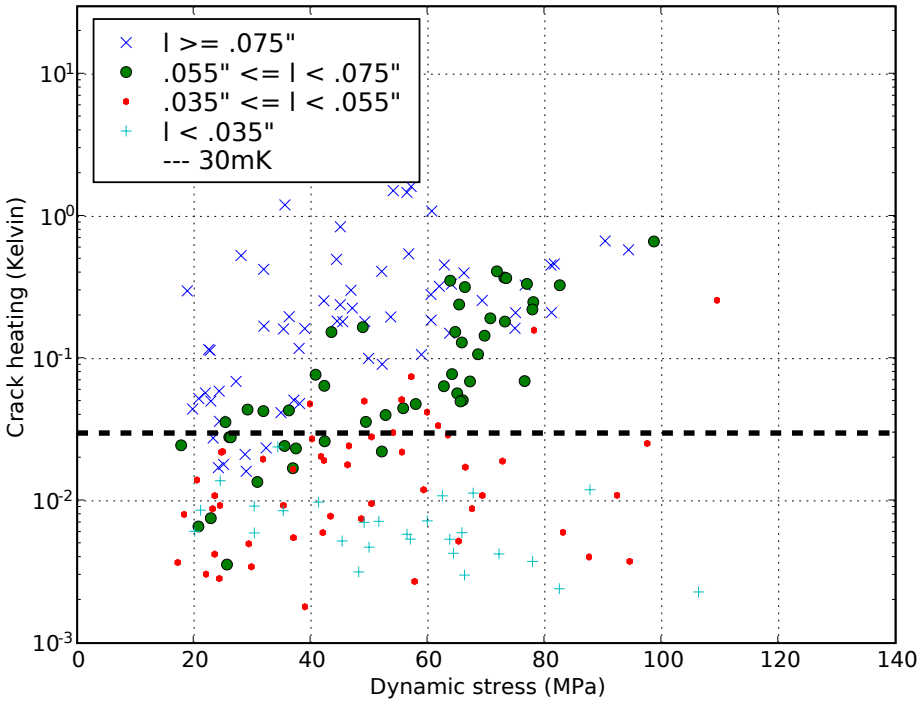

Figure 3.3 Crack heating versus dynamic stress for different crack lengths in titanium, resonant frequencies only, ISU 10/23/07.

of stress that must be applied to a crack of given size in order to cause it to heat. This is the first step to a direct relationship between crack heating and the physical quantities of the crack. Physical quantities of crack length and applied stress are required for any meaningful vibrothermography crack detection study. By considering the relationship between applied stress and crack size we can begin to consider how much stress it would take to make cracks of any particular size detectable.

Next we consider Figure 3.4 which shows crack heating as a function of crack length in titanium. Stress values are now separated into four ranges as shown. Again we see that regardless of crack size the higher stresses tend to cause more heating. We also observe that larger cracks tend to heat up more than smaller cracks in the detectable range. It remains clear that the larger cracks do not heat up when stress levels are too low. This again suggests a relationship between the quantities of crack heating, crack size, and applied stress.

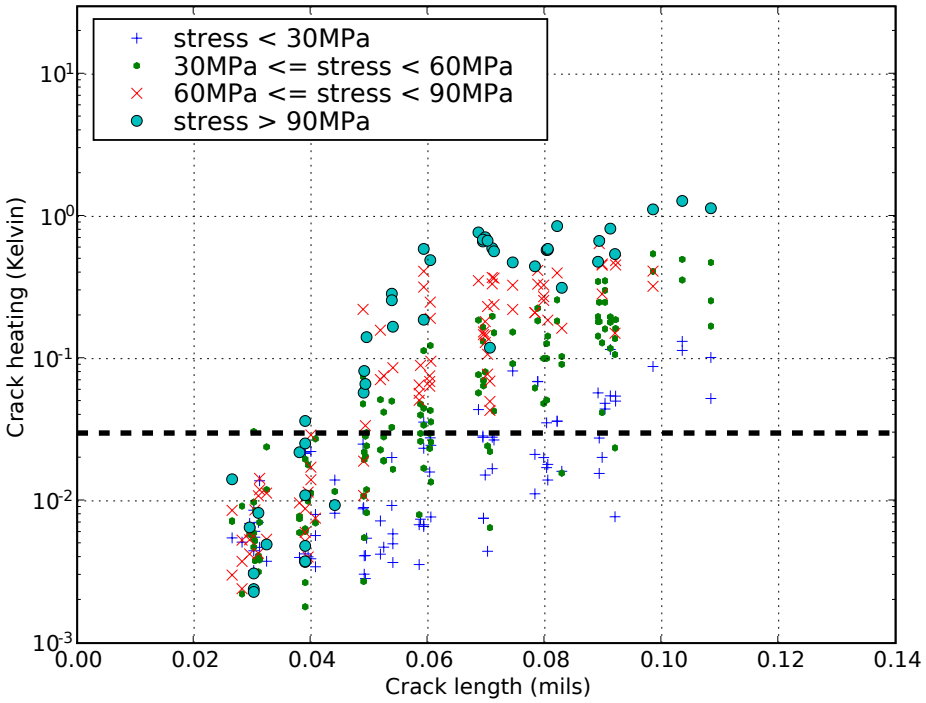

Figure 3.4 Crack heating versus crack length for different dynamic stress values in titanium, ISU 10/23/07.

Viewing this data in a 3D space provides more insight to the relationship between crack heating, crack size, and applied stress. Figure 3.5 shows a surface fit along with all data points. This surface fit was made by applying the power law to all data points above the detectable threshold and optimizing to find the best fit. The bright yellow points represent detectable heat values and the gray points fall below the detectable threshold. Again we note that a disproportionate number of points are colored gray but this is caused by the fact that half of the excitations were off resonance. Most off resonant excitations do not excite sufficient vibrational stress to cause detectable crack heating. The surface shows the detectable region in red and the non-detectable region in shadowed gray.

The 3D plot is shown from three different sides to give a sense of perspective. Figure 3.7 shows heating versus crack length from the front of the 3D space.

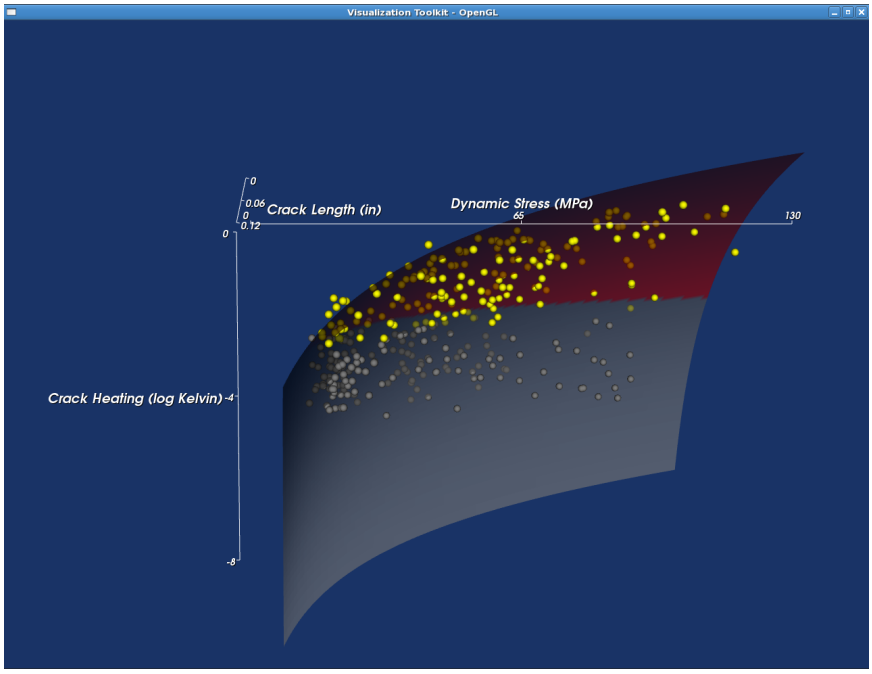

Figure 3.5 3D plot of crack detectability data shown with heating versus stress at the front. Titanium, ISU 10/23/07

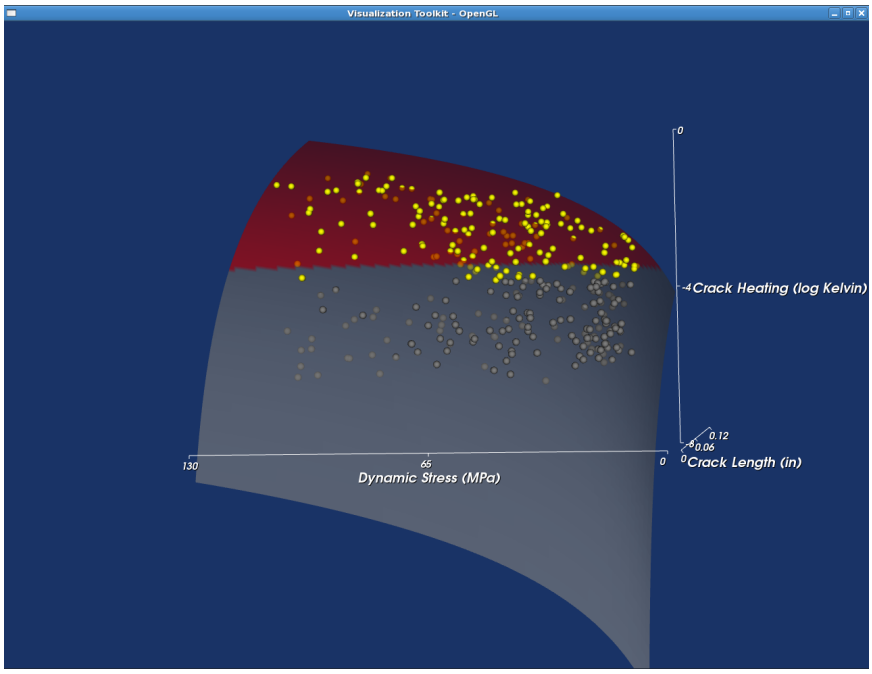

Figure 3.6 3D plot of crack detectability data shown with heating versus stress at the back. Titanium, ISU 10/23/07

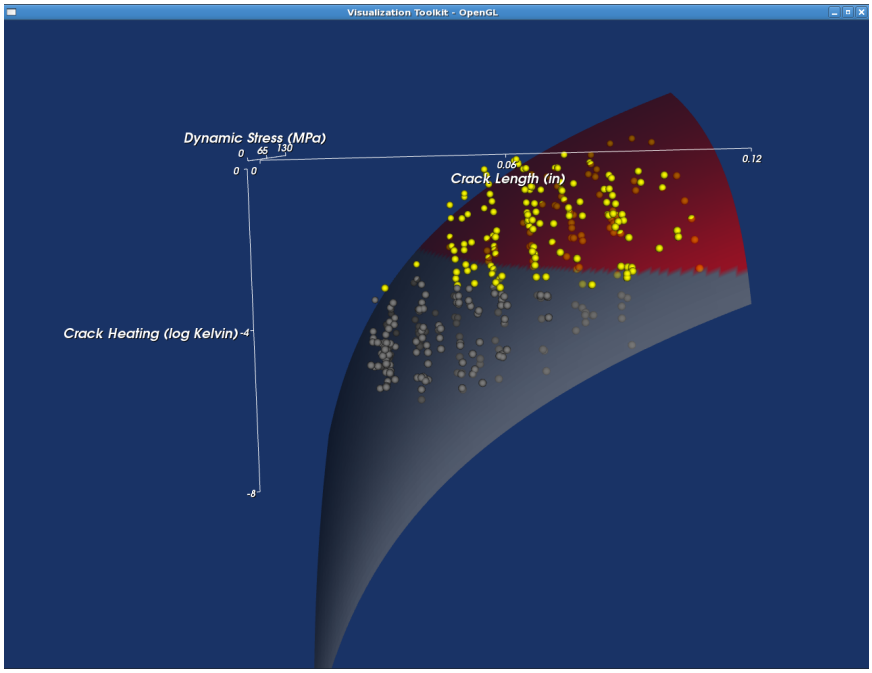

Figure 3.7 3D plot of crack detectability data shown with heating versus crack length at the front. Titanium, ISU 10/23/07

3.3 Inconel Sample Set

The Inconel sample set was tested in the same way as the titanium. Figure 3.8 shows crack heating as a function of applied stress for the entire Inconel sample set. First we notice that there are more points clustered at low dynamic stresses than there were in the titanium. This is caused by the wide distribution of resonant frequencies in the Inconel sample set. Because more samples were off the nominal frequency of 20070 Hz we see that more data points fall in the low stress region.

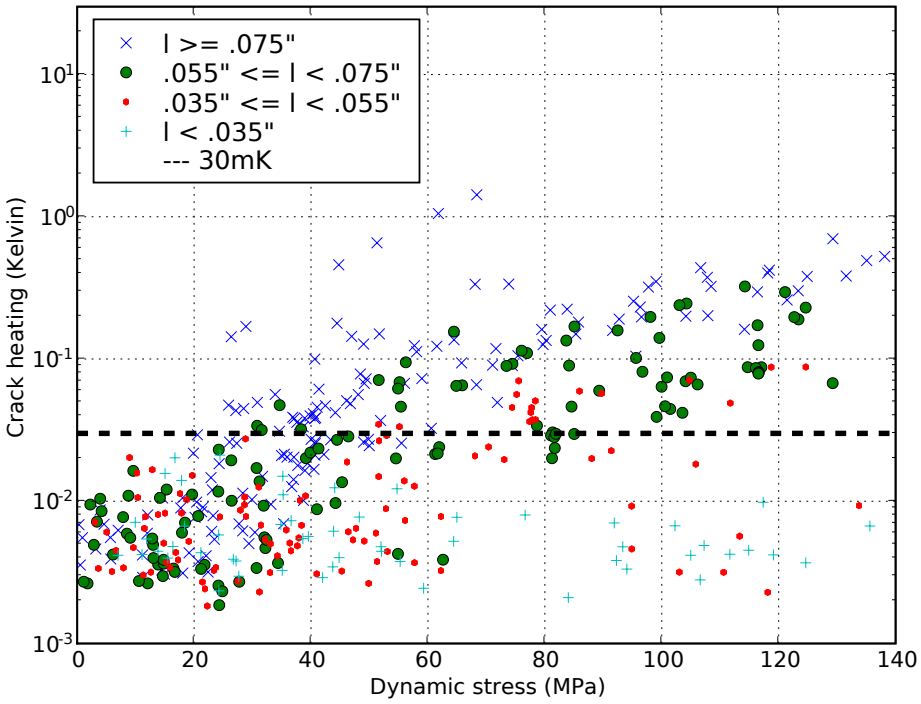

Figure 3.8 Crack heating versus dynamic stress for different crack lengths in Inconel, ISU 02/11/08.

Because the distribution of resonant frequencies in Inconel is not as tight we see a more pronounced shift when nominal frequency excitations are filtered out as in Figure 3.9. Most of the points below 30 MPa come from excitations off resonant frequency. This is a good indication of the importance of excitation at resonance. By using the natural motion of the

specimen we are able to get significantly more vibration with the same electrical power input. We have observed that dynamic stress still correlates to crack heating when excited slightly off resonance .

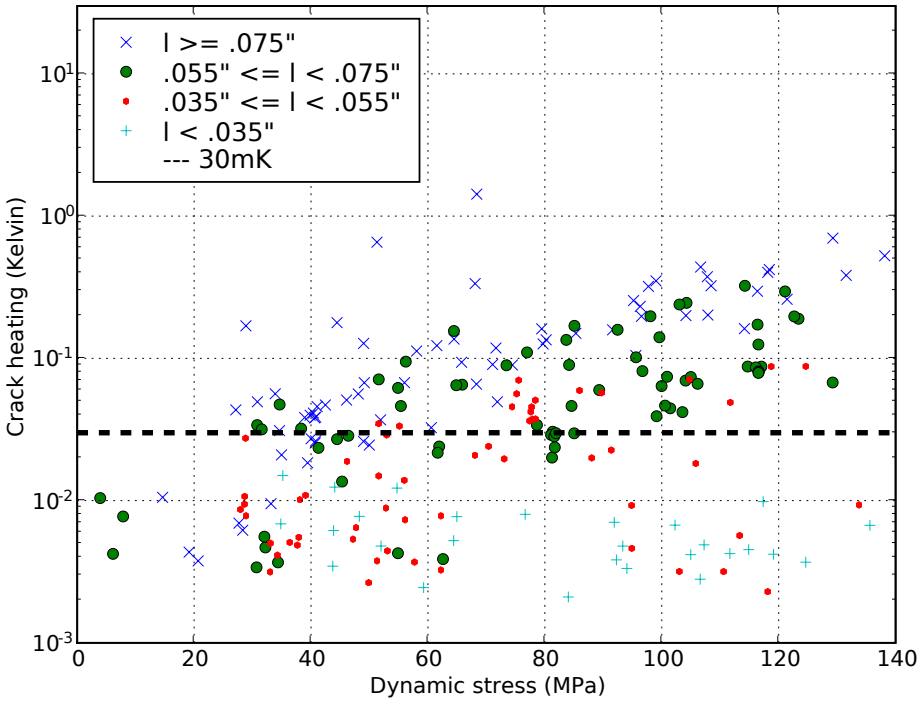

Figure 3.9 Crack heating versus dynamic stress for different crack lengths in Inconel taking only hits at resonant frequency, ISU 02/11/08.

Figure 3.10 shows crack heating as a function of crack length for a range of dynamic stress values in Inconel. Again two trends are clear. Higher applied stresses lead to higher heating values and larger cracks heat up more. We also see that in Figure 3.10 the crack lengths fall into relatively distinct columns. These cracks were grown to specific target lengths under controlled conditions so there are distinct blocks of lengths. This partitioning of crack lengths was more noticeable in Inconel that it was in titanium.

Again 3D representation of this data in Figures 3.11, 3.12, and 3.13 provides insight to the relationship between crack heating, dynamic stress, and crack length. In Inconel we observe a relationship between crack heating, dynamic stress, and crack length that is similar to the

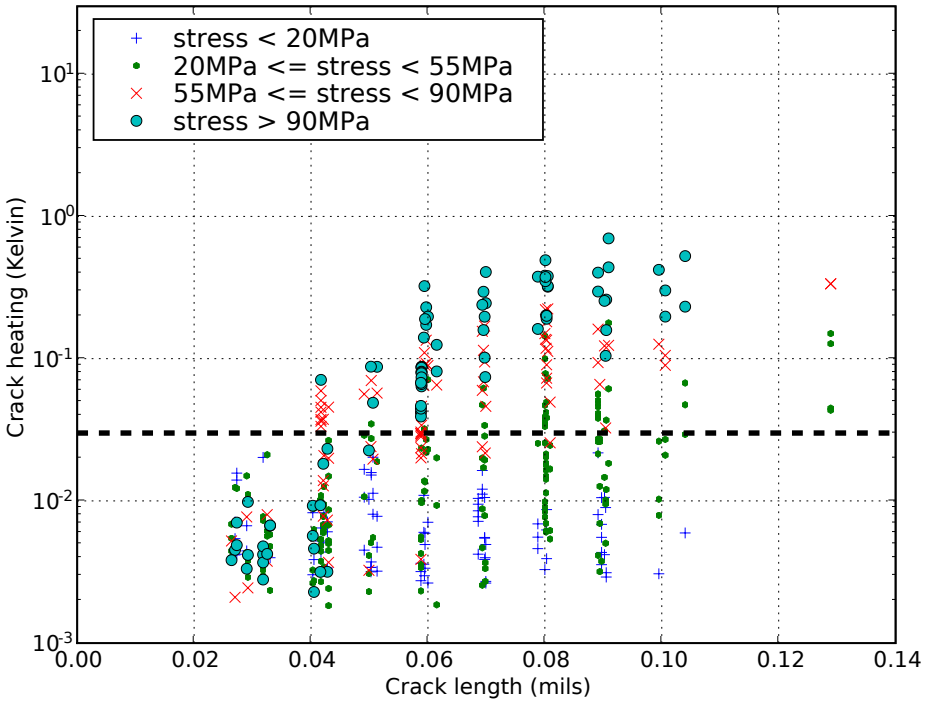

Figure 3.10 Crack heating versus crack length for different dynamic stress values in Inconel, ISU 02/11/08.

relationship for titanium. One difference between titanium and Inconel data is the stress required for crack detectability. We see less detectability in Inconel than in titanium at stress values below 60MPa. This is caused by the fact that Inconel is nearly twice as stiff as titanium. Higher stiffness means more force is required to cause the same amount of motion. More force means higher stresses.

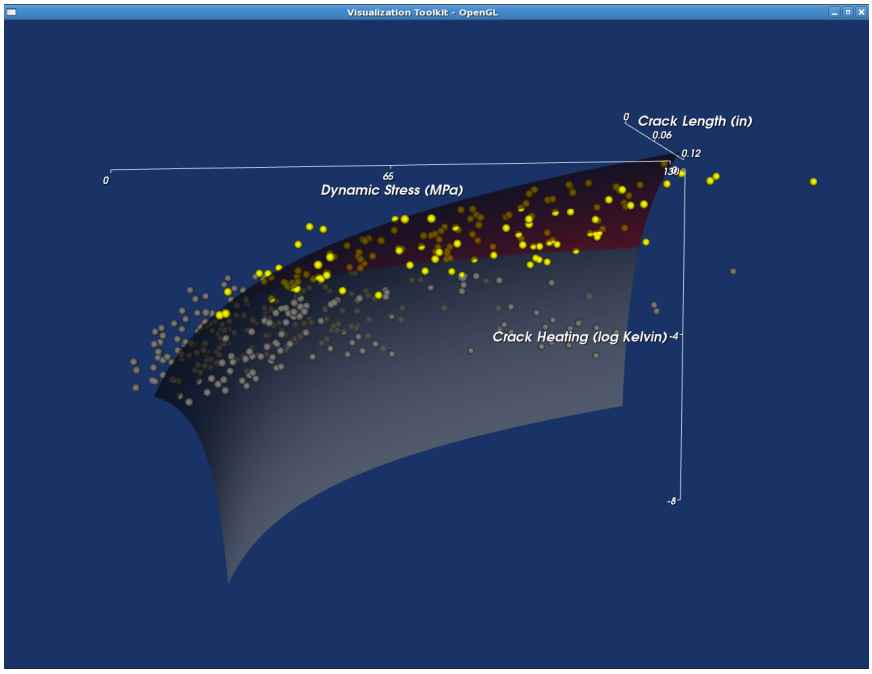

Figure 3.11 3D plot of crack detectability data shown with heating versus stress at the front. Inconel, ISU 02/11/08

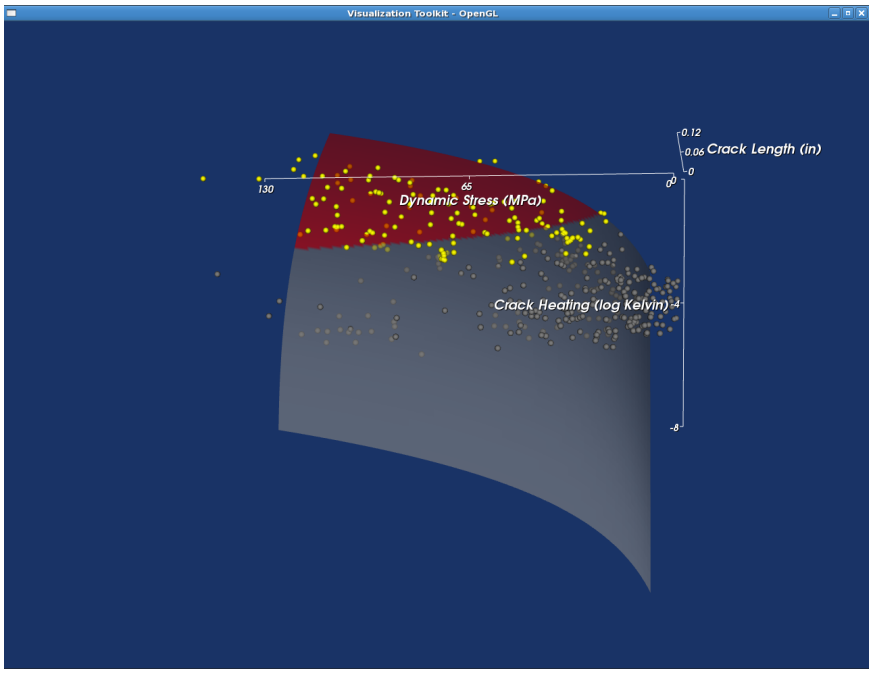

Figure 3.12 3D plot of crack detectability data shown with heating versus stress at the back. Inconel, ISU 02/11/08

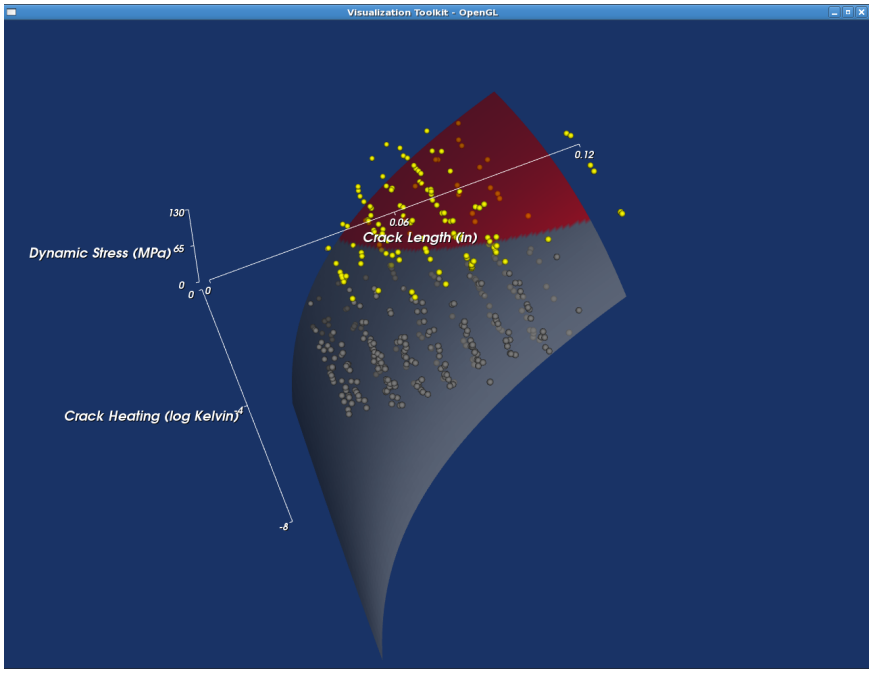

Figure 3.13 3D plot of crack detectability data shown with heating versus crack length at the front. Inconel, ISU 02/11/08

3.4 Conclusion

We have shown that the use of a tunable, resonant excitation provides a repeatable linear vibration response. Known vibration modes make it possible to extract the dynamic vibrational stress at a crack using a single point vibrometer measurement. These resonant modes have deformed shapes and frequencies that can be calculated from theory and numeric simulation. Theoretical and numeric calculations match measured mode shapes for these samples. Understanding the vibration modes present in a sample allows us to tune a particular mode to a desired frequency.

From a known resonance the stress is calculated using measured surface velocity and the known mode shape. When we relate the stress to crack heating we observe the dependence of crack heating on crack size and vibrational stress. Without adequate vibrational stress no heating is observed. The heating relationship further shows that detecting smaller cracks requires greater vibrational stresses. As the applied stress increases so does the crack heating likewise as crack length increases so does the crack heating. This correlation shows that at a given crack length a minimum applied dynamic stress is needed for a high probability of detectable crack heating. Finally, we show that the higher vibrational stresses achieved through resonant testing also correlate with larger amounts of crack heating. Thus, directly relating crack heating to the applied stress on a crack corrects for excitation variability. Understanding the stresses that result from the vibration response isolates one variable from the crack heating relationship. The relationship between crack heating, crack size, and vibrational stress will be useful for extrapolating crack detectability from test specimens to useful parts such as actual turbine components.

APPENDIX A. ANSYS SCRIPT

```
/prep7
et,1,92
mp,ex,1,113.8e9
mp,nuxy,1,.342
mp,dens,1,4.42e3
block,0,0.155,0,0.0255,0,0.0125
asel,all
aesize,all,.004
vmesh,all
finish
/solu
antype,modal
modopt,lanb,20,1000,50000
solve
finish
/post1
/view,,1,1,1
/replot
/color,wbak,0
/color,outl,0
set,1,6
pldisp,0
```

APPENDIX B. ANSYS RESULTS

***** INDEX OF DATA SETS ON RESULTS FILE *****

SET	TIME/FREQ	LOAD STEP	SUBSTEP	CUMULATIVE	Vibration Mode
1	2654.4	1	1	1	First flexural
2	5076.5	1	2	2	First sideways flexural
3	7045.2	1	3	3	Second flexural
4	7338.4	1	4	4	First torsional
5	12342.	1	5	5	Second sideways flexural
6	13141.	1	6	6	Third flexural
7	14730.	1	7	7	Second torsional
8	16341.	1	8	8	First extensional
9	20491.	1	9	9	Fourth flexural
10	21156.	1	10	10	Third sideways flexural

BIBLIOGRAPHY

[1] C. Homma, M. Rothenfusser, J. Baumann, R. Shannon, "Study of the heat generation mechanism in acoustic thermography," in *Review of Progress in Quantitative Nondestructive Evaluation*, edited by D. O. Thompson and D. E. Chimenti, AIP Conference Proceedings vol. 25, American Institute of Physics, Melville, NY, pp. 566-573 (2006).

[2] J. DiMambro, D.M. Ashbaugh, C.L. Nelson, and F.W. Spencer, "Sonic Infrared (IR) Imaging and Fluorescent Penetrant Inspection Probability of Detection (POD) Comparison," in *Review of Progress in Quantitative Nondestructive Evaluation 26* , edited by D. O. Thompson and D. E. Chimenti, AIP Conference Proceedings vol. 894, American Institute of Physics, Melville, NY, pp. 463-470 (2007).

[3] M. W. Burke, W. O. Miller, "Status of VibroIR at Lawrence Livermore," in *Thermosense XXVI Proc. SPIE*, Vol. 5405, pp. 313-321 (2004).

[4] M. Rothenfusser, C. Homma, "Acoustic thermography: vibrational modes of cracks and the mechanism of heat generation," in *Review of Progress in Quantitative Nondestructive Evaluation*, edited by D. O. Thompson and D. E. Chimenti, AIP Conference Proceedings vol. 24, American Institute of Physics, Melville, NY, pp. 624-631 (2005).

[5] S. D. Holland, C Uhl, and J. Renshaw "Toward a viable strategy for estimating vibrothermographic probability of detection," in *Review of Progress in Quantitative Nondestructive Evaluation*, edited by D. O. Thompson and D. E. Chimenti, AIP Conference Proceedings, American Institute of Physics, Melville, NY, in press.

[6] Xiaoyan Han, Zhi Zeng, Wei Li, Md. Sawar Islam, Jianping Lu, Vera Loggins, E. Yitamben, L. D. Favro, G. Newaz, R. L. Thomas, "Acoustic chaos for enhanced detectability of

cracks by sonic infrared imaging," in *Journal of Applied Physics*, Vol. 95, No. 7, 3792-3797 (2004).

[7] J. Renshaw and S. D. Holland, "Full-field vibration measurement for vibrothermography," in *Review of Progress in Quantitative Nondestructive Evaluation*, edited by D. O. Thompson and D. E. Chimenti, AIP Conference Proceedings, American Institute of Physics, Melville, NY, in press.

[8] S. D. Holland, J. Renshaw, R. Roberts, "Measurement of dynamic full-field internal stresses through surface laser Doppler vibrometry," *Appl. Phys. Letters*, in press.

[9] Key Words: Titanium 6-4, Inconel 718, April 2008 http://www.matweb.com/search

[10] W. C. Elmore, M. A. Heald, *Physics of Waves*, Dover Publications Inc., New York, pp. 116-122